*Sensors & Transducers, Vol. 197, Issue 2, February 2016, pp. 78-86*

www.sensorsportal.com

**Sensors & Transducers**

© 2016 by IFSA Publishing, S. L.

*http://www.sensorsportal.com*

# Real-Time Vehicle Speed Estimation Based on License Plate Tracking in Monocular Video Sequences

**[1] Aleksej MAKAROV, [2] Vojislav LUKIĆ and [1] Bhaskar CHOUBEY**

[1] University of Oxford, Department of Engineering, 17 Parks Road, Oxford, OX1 3PJ, UK

[2] Vlatacom d.o.o., Bulevar Milutina Milankovića 5, 11070 Novi Beograd, Serbia

[1] Tel.: +44 (0) 1865 273096, fax: +44 (0) 1865 273010

[1] E-mail: aleksej.makarov@eng.ox.ac.uk

*Received: 6 January 2016 /Accepted: 29 January 2016 /Published: 29 February 2016*

**Abstract:** A method of estimating the vehicle speed from images obtained by a fixed over-the-road monocular camera is presented. The method is based on detecting and tracking vehicle license plates. The contrast between the license plate and its surroundings is enhanced using infrared light emitting diodes and infrared camera filters. A range of the license plate height values is assumed *a priori*. The camera vertical angle of view is measured prior to installation. The camera tilt is continuously measured by a micro-electromechanical sensor. The distance of the license plate from the camera is theoretically derived in terms of its pixel coordinates. Inaccuracies due to the frame rate drift, to the tilt and the angle of view measurement errors, to edge pixel detection and to a coarse assumption of the vehicle license plate height are analyzed and theoretically formulated. The resulting system is computationally efficient, inexpensive and easy to install and maintain along with the existing ALPR cameras. *Copyright © 2016 IFSA Publishing, S. L.*

**Keywords:** Machine vision metrology, Error analysis, Speed estimation, Monocular stereoscopy, Statistical calibration.

## 1. Introduction

Measuring speed of vehicles on a highway is an important and frequent task in traffic security. Inappropriate speed contributes to 14 % of all injuries, 15 % of serious injuries and 24 % of deaths on the road. By 2020, road traffic crashes are expected to move from the ninth to the third-ranked cause of disability [1-4].

Various speed measurement systems have been developed over several decades, ranging from piezo-sensors, magnetic stripes and inductive loops embedded in pavement to LIDAR speed guns and radars. These systems are mostly used in stationary and autonomous settings.

An independent speed measurement check is often desirable for legal and calibration purposes. In UK, for example, the law stipulates that one speed estimate is insufficient without corroboration (Section 89(2) Road Traffic Regulation Act 1984), which can be provided by a device whose accuracy and reliability can be established. Secondary estimates should be within ±10 % of the primary measurements [5].

Stationary traffic speed measurement devices are integrated with cameras in order to provide a visual evidence of the vehicle and driver identity. Using a camera should therefore provide a straightforward source of corroborative measurements.

Though machine vision is often used in metrology, its application to vehicle speed

measurements is hampered by adverse conditions encountered in the road traffic environment. The latter include variable lighting and weather conditions, poor contrast between vehicle tires and the road surface as well as camera calibration uncertainties due to mechanical vibrations and shocks.

In practice, these difficulties are overcome by using camera calibration lines painted on the road surface [6, 7]. However, these road markings are subject to wear and require undesirable carriageway closures when repainted.

Camera-based traffic speed meters which do not require road closures during their installation or maintenance have been reported in the literature [10-13]. These methods are based on edge extraction and localization of vanishing points [10], on statistical assumptions on vehicle dimensions [11, 12] or on binocular stereoscopic measurements [13]. However, these methods present some drawbacks when applied in practice.

Binocular systems are more expensive due to the doubled cost of cameras. Disparity and depth maps involve computationally expensive techniques over a significant number of pixels. Speed measurements require satisfactory synchronization between sensors, which is a rather non-trivial issue with off-the-shelf cameras. Finally, the acceptable speed measurements errors of less than 10 % require baselines exceeding 0.5 meters, resulting in cumbersome systems requiring additional installation effort [13].

Vanishing point based [10] and statistical methods [11, 12] use monocular cameras and involve an initial period of self-calibration. This period is used for finding orthogonal vanishing points. The localization of vanishing points is known to depend on the quality of extracted edges, which can be a problem in low-contrast environments. Speed estimates require good segmentation of vehicles, which also depends on the contrast between the vehicle and its surroundings.

The system presented in this paper overcomes the segmentation and edge detection issues due to low contrast by using infrared illumination and infrared filters. Instead of segmenting vehicles, only license plates are extracted. This step is common in many contemporary systems which employ automated license plate recognition (ALPR). The plate extraction is facilitated due to infrared reflective coating, nowadays a standard on all European, American and Australian license plates, providing high contrast with respect to the uncoated surroundings. The method is computationally simple and does not necessitate the localization of edges other than horizontal license plate rims. The underlying assumption is related to a legally and practically limited range of license plate heights with respect to the ground.

This paper is organized as follows. Section 2 describes the mathematical foundation of the image-based speed estimation method. Section 3 analyzes different sources of error affecting the method and demonstrates the feasibility of image-based speed estimation for traffic law enforcement purposes.

## 2. Estimating the License Plate Position and Speed

Measuring the speed of a vehicle using a camera involves scene calibration, which in turn requires the camera parameters, such as the tilt and the angle of view to be known in advance. For simplicity, the camera will be assumed to be mounted over the carriageway. In this case, the parameters of interest are:

- The tilt of the camera with respect to the road, $\alpha$,
- The vertical angle of view $\phi$ and
- The camera height with respect to the tracked feature *h*. which is, in our case, the lower edge of the license plate.

These parameters are illustrated in Fig. 1. Note that the camera mounting height *H* above the ground is fixed, while the camera height above the license plate lower edge *h* is variable and depends on the mounting height of the license plate on a vehicle.

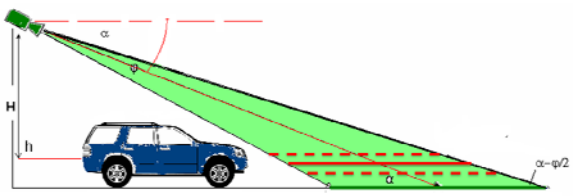


**Fig. 1.** Tilt $\alpha$, vertical angle of view $\phi$ and the height of the camera with respect to the license plate *h*. Dashed lines shown inside the field of view correspond to the range of heights of the lower license plate edge. The solid red line in between represents the assumed height of the license plate.

While the camera tilt and the vertical angle of view can be precisely mesured, the camera height with respect to the vehicle license plate depends on the vehicle model, i.e., on the height above the ground at which the license plate is fixed to a vehicle. The latter varies within limits which will be described in the next section. Fig. 2 illustrates different license plate heights with respect to the ground.

**Fig. 2.** License plates occur at different heights, but within the range between 30 and 110 centimeters above the ground.

The speed of a vehicle moving on a short segment of a lane can be estimated from its longitudinal displacement along the horizontal axis shown in Fig. 1 (solid red line). The precise values of the tilt $\alpha$ and the vertical angle of view $\phi$ can be measured in advance, as well as the height $H$ of the camera with respect to the ground. An assumption about the vertical distance $h$ between the camera and the license plate lower edge can be made based on the legally restricted license plate height range defined in [14]. From $\alpha$, $\phi$ and $h$ the license plate position R can be assessed, as illustrated in Fig. 3.

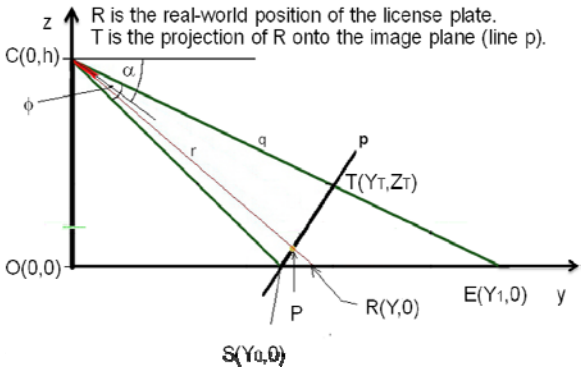


**Fig. 3.** Computing the real-world position **R** of the license plate lower edge on *y* axis from the camera tilt, angle of view and the assumed relative height of the camera with respect to R.

The following steps can be implemented in order to analytically express the longitudinal position Y of the vehicle license plate to its image projection coordinates and parameters $\alpha$, $\phi$ and $h$:

1) Find the point $S(Y_0,0)$ where the license plate edge enters the image plane;

2) Find the point $E(Y_1,0)$ where the license plate exits the image plane;

3) Find the straight-line equation for ray $q$, connecting the camera with $E(Y_1,0)$

4) Find the straight-line equation for the intersection $p$ of the image plane and the yOz plane.

5) Compute the real-world coordinates of point T in the image plane, to which $E(Y_1,0)$ projects. An alternative way to find this point is by noting that it is a vertex of the isosceles triangle CST, hence its distance from the camera (point C) is the same as the distance of the point of entry of the lower plate edge into the scene (point S).

6) Partition the image plane into $N_r$ equal stripes (i,e,, the line segment ST into $N_r$ equal intervals), where $N_r$ is the number of rows in the image sensor. Enumerate the stripes from 1 at the top (enclosing point T) to $N_r$ at the bottom (enclosing point S).

7) Find the point P in the image plane corresponding to the row $n_r$ which contains the lower edge of the license plate in the image.

8) Find the straight-line equation of ray r connecting the camera (point C) and the point P.

9) Find the real-world position of the lower license plate edge (point R) at the intersection of the ray r and y axis.

The above steps are analytically expressed in the paragraphs hereafter.

## 2.1. Point of Entrance into the Field of View

Point of entrance of the license plate lower edge into the field of view is here defined as a point at the intersection of the vertical yOz plane, containing the optical axis of the camera, and the horizontal line at the height corresponding to the assumed vertical position of the license plate lower edge, i.e., the y-axis. In Fig. 3, the angle OPC is on the opposite side of the transversal CS to the sum of the tilt and the vertical field of view of the camera $\alpha+\phi/2$, and hence equal to it. Consequently,

$$Y_0 = h \cdot \cot(\alpha + \frac{\varphi}{2}) \tag{1}$$

## 2.2. Point of Exit from the Field of View

Similarly, the angle OEC is on the opposite of the transversal q to $\alpha-\phi/2$, giving the furthest longitudinal distance from the camera where the license plate lower edge can still be observed,

$$Y_1 = h \cdot \cot(\alpha - \frac{\varphi}{2}) \tag{2}$$

## 2.3. Exit Ray Equation

The straight-line equation for ray q passing through the sensor at C and through the exit point E in Fig. 3 is therefore

$$z_q = -\tan(\alpha - \frac{\varphi}{2}) \cdot y + H \tag{3}$$

## 2.4. Intersection of the Image Plane with the Longitudinal (yOz) Plane

The line p is parallel to the sensor plane, i.e., contained in the image plane. It is located at the intersection between the image plane and the yOz plane illustrated in Fig. 3. The line p can be obtained by observing the angle T'ST, where T' is the orthogonal projection of the point T onto y axis, as shown in Fig. 4. This angle is equal to $\pi/2-\alpha$, as deduced from the right triangle ST'T and the lines of angle T'TS perpendicular to the optical axis (dashed) and the horizontal line drawn from C.

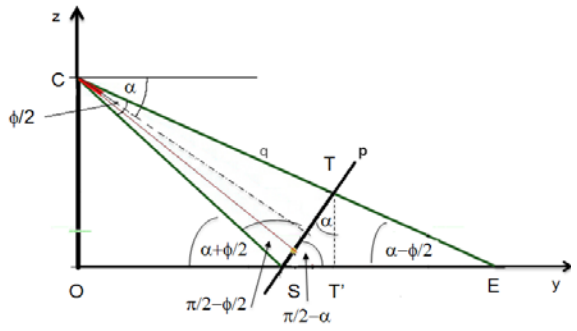


**Fig. 4.** Computing the real-world position **R** of the license plate lower edge on *y* axis from the camera tilt, angle of view and the assumed relative height of the camera with respect to R.

Therefore, the line equation for p is

$$z = \cot(\alpha)\cdot y - Y_0\cot(\alpha) \tag{4}$$

i.e.

$$z_p = \cot(\alpha)\cdot y - \cot(\alpha)\cdot\cot(\alpha+\frac{\varphi}{2})\cdot H \tag{5}$$

## 2.5. Point of Intersection of the Exit Ray with the Image Plane

Point T is a point in the middle of the top row of the image. It lies at the intersection of lines p and q. From $z_p$=$z_q$,

$$Y_T = h\cdot\frac{1+\cot\left(\alpha+\frac{\varphi}{2}\right)\cdot\cot(\alpha)}{\cot(\alpha)+\tan\left(\alpha-\frac{\varphi}{2}\right)} \tag{6}$$

and

$$Z_T = h\cdot\cot(\alpha)\cdot\frac{1-\cot\left(\alpha+\frac{\varphi}{2}\right)\tan\left(\alpha-\frac{\varphi}{2}\right)}{\cot(\alpha)+\tan\left(\alpha-\frac{\varphi}{2}\right)} \tag{7}$$

## 2.6. Partition of the Image Plane into Rows

The image plane in Fig. 3 is represented by its intersection with the yOz plane, which is the line p. Since points S and T on line p are known, the line segment ST can be partitioned into $N_r$ equal intervals.

$$Y_n = Y_0 + \frac{N_r - n}{N_r}\cdot\left(Y_T - Y_0\right) \tag{8}$$

and

$$Z_n = \frac{N_r - n}{N_r}\cdot Z_T \tag{9}$$

where n={0, 1, 2, … , $N_r - 1$}, counting from the top to the bottom row of the image.

## 2.7. Relationship between a Real-world Position of a Feature and its Image Row

Any feature intersecting with ray r occupies a pixel in row $n_p$, as shown in Fig. 3. Rows are counted from the top of the image, i.e., from the point T, towards the bottom, i.e., point S. Row $n_p$ corresponds to projections onto point P in the image plane, whose real-world coordinates of interest are

$$Y_P = Y_0 + \frac{N_r - n_p}{N_r}\cdot\left(Y_T - Y_0\right) \tag{10}$$

and

$$Z_P = \frac{N_r - n_p}{N_r}\cdot Z_T \tag{11}$$

## 2.8. Projection Ray Equation

The feature of interest, the lower edge of the license plate of a vehicle is assumingly located on y-axis, at its intersection with ray r. This ray runs through points C (the camera) and P (projection of a point at the license plate edge onto the image plane). From Fig. 3, the ray r can be expressed as

$$z_r = \frac{Z_P - h}{Y_P}y + h \tag{12}$$

## 2.9. Real-world Position of the License Plate

The intersection of the projection ray r with y-axis (z=0) is the point R where the lower edge of the license plate is assumed to be located. Point R lies at horizontal distance $Y_R$ from the camera,

$$Y_R = \frac{h\cdot Y_P}{h - Z_P} \tag{13}$$

Expressed in camera parameters, the horizontal distance between the camera and the plate is

$$Y_R = h\cdot\ldots\frac{\left(2-\frac{n_p}{N_r}\right)\cos\left(\alpha+\frac{\varphi}{2}\right)-\left(1-\frac{n_p}{N_r}\right)\cos\left(\alpha-\frac{\varphi}{2}\right)}{\frac{n_p}{N_r}\cdot\sin\left(\alpha+\frac{\varphi}{2}\right)+\left(1-\frac{n_p}{N_r}\right)\cdot\sin\left(\alpha-\frac{\varphi}{2}\right)} \tag{14}$$

### 2.10. Speed Estimation

Assuming the position $Y_R$ observed at two different times, $t_1$ and $t_2$, the speed estimate is obtained as

$$v_R(t_2) = \frac{Y_R(t_2) - Y_R(t_1)}{t_2 - t_1} \tag{15}$$

or, in terms of the frame rate $f$ and frame numbers $m_i$,

$$v_R(m_2) = f\,\frac{Y_R(m_2) - Y_R(m_1)}{m_2 - m_1} \tag{16}$$

## 3. Error Sources

Equations (14) and (16) express the estimates of the vehicle position and speed at different time instants. The variables occurring in these equations are the camera tilt $\alpha$, the vertical field of view $\phi$, the position of the lower edge of the license plate within the image (i.e., the row number $n_r$ with respect to the total number of rows $N_r$), the height of the camera with respect to the license plate $h$ and the frame rate $f$. Errors in estimating these variables produce a speed estimation error whose limits are derived in this section.

### 3.1. Tilt

Tilt sensors, or inclinometers, based on micro electro-mechanical systems (MEMS) technology are suitable for controlling the camera tilt in image-based distance and speed measurements. For instance, the SCA103T series has the measurement range of 30° and accuracy of 0.001°. From Equation (14), the partial derivative of $Y_R$ with respect to tilt is

$$\frac{\partial Y_R}{\partial \alpha} = h \cdot \ldots$$
$$\frac{2\cdot\left(\frac{n_P}{N_r}\right)^2 - 4\cdot\frac{n_P}{N_r} + 1 - 2\cdot\left(1-\frac{n_P}{N_r}\right)^2\cos\varphi}{\left[\frac{n_P}{N_r}\cdot\sin\left(\alpha+\frac{\varphi}{2}\right)+\left(1-\frac{n_P}{N_r}\right)\cdot\sin\left(\alpha-\frac{\varphi}{2}\right)\right]^2} \tag{16}$$

The contribution of the tilt error to the positioning relative error is therefore

$$\frac{1}{Y_R}\left|\frac{\partial Y_R}{\partial\alpha}\right|\delta\alpha = \frac{\delta\alpha}{\frac{n_P}{N_r}\cdot\sin\left(\alpha+\frac{\varphi}{2}\right)+\left(1-\frac{n_P}{N_r}\right)\cdot\sin\left(\alpha-\frac{\varphi}{2}\right)}\cdot$$
$$\cdot\frac{2\cdot\left(1-\frac{n_P}{N_r}\right)^2\cdot\cos\varphi - 2\cdot\left(\frac{n_P}{N_r}\right)^2 + 4\cdot\frac{n_P}{N_r} + 1}{\left(2-\frac{n_p}{N_r}\right)\cos\left(\alpha+\frac{\varphi}{2}\right)-\left(1-\frac{n_p}{N_r}\right)\cos\left(\alpha-\frac{\varphi}{2}\right)} \tag{17}$$

The graph in Fig. 5 shows how the relative error caused by the tilt inaccuracy varies with the image row. The tilt error was assumed to be $\delta\alpha$=0.001°.

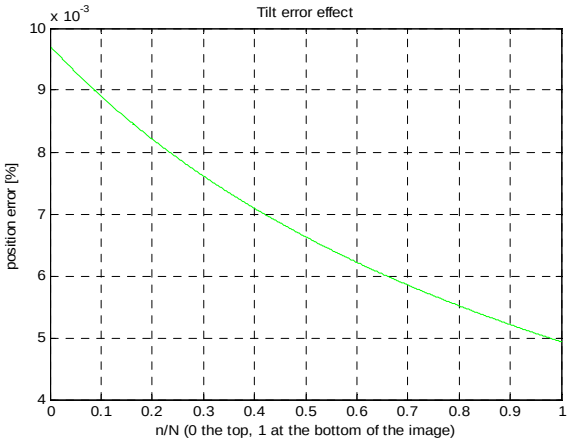


**Fig. 5.** The positioning error due to the tilt inaccuracy according to Equation (17) increases towards the top of the image.

### 3.2. Angle of View

The vertical angle of view of a camera can be determined in the laboratory conditions prior to mounting. The method described in [15] has been used with the resulting error of $\delta\alpha$=0.1°. The analytical expression for the contribution of the field-of-view error is

$$\frac{\partial Y_R}{\partial\varphi} = h\times$$
$$\times\frac{2\cdot\left(1-\frac{n_P}{N_r}\right)\cdot\cos(2\alpha)-1}{2\cdot\left[\frac{n_P}{N_r}\cdot\sin\left(\alpha+\frac{\varphi}{2}\right)+\left(1-\frac{n_P}{N_r}\right)\cdot\sin\left(\alpha-\frac{\varphi}{2}\right)\right]^2} \tag{18}$$

The contribution of the field-of-view inaccuracy to the positioning relative error is

$$\frac{1}{Y_R}\left|\frac{\partial Y_R}{\partial\varphi}\right|\delta\varphi = \frac{\left|1-2\cdot\left(1-\frac{n_P}{N_r}\right)\cdot\cos(2\alpha)\right|}{2\cdot\left[\frac{n_P}{N_r}\cdot\sin\left(\alpha+\frac{\varphi}{2}\right)+\left(1-\frac{n_P}{N_r}\right)\cdot\sin\left(\alpha-\frac{\varphi}{2}\right)\right]}\cdot$$
$$\cdot\frac{\delta\varphi}{\left(2-\frac{n_p}{N_r}\right)\cos\left(\alpha+\frac{\varphi}{2}\right)-\left(1-\frac{n_p}{N_r}\right)\cos\left(\alpha-\frac{\varphi}{2}\right)} \tag{19}$$

The graph in Fig. 6 shows how the relative error caused by the vertical field-of-view inaccuracy varies over image rows for $\delta\alpha$=0.1°.

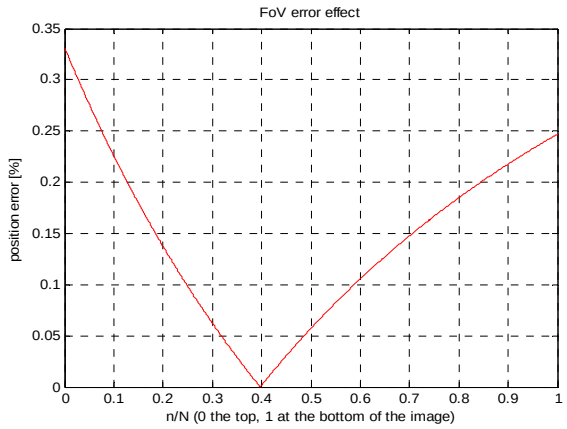


**Fig. 6.** The positioning error due to the field-of-view inaccuracy according to Equation (19) decreases towards the centre, then increases towards the top of the image.

### 3.3. Error in Image Coordinates of an Edge Pixel

The license plate edges may be incorrectly extracted due to noise, defective pixels, poor contrast or biased edge extractors. This error is usually within one pixel of the "true" image row to which an edge should have been assigned. The analytical expression for the contribution of the image row error is derived hereafter, where for the sake of simplicity, the row number $n$ is assumed to continuously vary between 0 and $N_r$,

$$\frac{\partial Y_R}{\partial n} = h \cdot \ldots \frac{(-2)\cdot \sin\left(\frac{\varphi}{2}\right)\cos\left(2\alpha+\frac{\varphi}{2}\right)}{\left[\frac{n_P}{N_r}\cdot\sin\left(\alpha+\frac{\varphi}{2}\right)+\left(1-\frac{n_P}{N_r}\right)\cdot\sin\left(\alpha-\frac{\varphi}{2}\right)\right]^2} \quad (20)$$

The contribution of the row number error to the positioning relative error is therefore

$$\frac{1}{Y_R}\left|\frac{\partial Y_R}{\partial n}\right|\delta n = \frac{2\sin\left(\frac{\varphi}{2}\right)\cdot\cos\left(2\alpha+\frac{\varphi}{2}\right)}{\frac{n_P}{N_r}\cdot\sin\left(\alpha+\frac{\varphi}{2}\right)+\left(1-\frac{n_P}{N_r}\right)\cdot\sin\left(\alpha-\frac{\varphi}{2}\right)} \cdot \frac{\delta n}{\left(2-\frac{n_p}{N_r}\right)\cos\left(\alpha+\frac{\varphi}{2}\right)-\left(1-\frac{n_p}{N_r}\right)\cos\left(\alpha-\frac{\varphi}{2}\right)} \quad (21)$$

The graph in Fig. 7 shows how the relative error in real-world positioning caused by inaccurate row numbering varies over the image for δn=1 pixel.

### 3.5. Height of the License Plate

The height of the license plate above the ground is subject to national traffic laws. While admissible plate height ranges differ across the globe, they all overlap in the interval adopted by EU countries [14]:

- The height of the lower edge of the plate from the ground surface shall not be less than 0.30 m.
- The height of the upper edge of the plate from the ground surface shall not exceed 1.20 m.

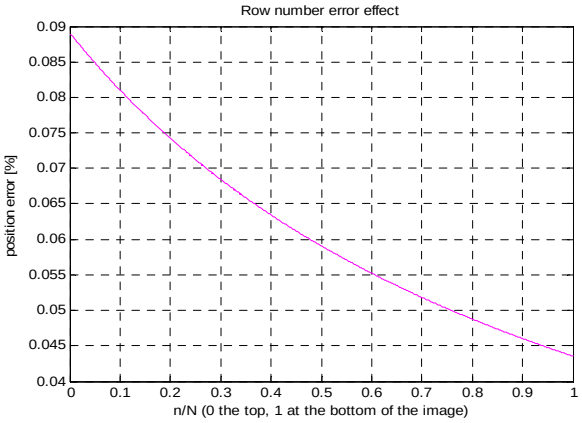


**Fig. 7**. The positioning error due to row number error according to Equation (21) increases towards the top of the image.

For simplicity, it is convenient to track only one horizontal edge of a license plate, assuming the vertical dimension $h_p$ of a license plate is known. Consequently, the height $H$-$h$ in Fig. 1, locating the lower edge of a license plate is limited by inequality (22),

$$H - h + h_p \le 1.20 \text{ m} \quad (22)$$

The vertical dimension $h_p$ of a license plate is also regulated by national traffic laws, but is never less than 10 cm. Consequently, the range of the lower edge height of a license plate is between the following limits,

$$H - h \le 1.10 \text{ m} \quad (23)$$

$$H - h \ge 0.30 \text{ m} \quad (24)$$

above the ground. From inequalities (2) and (3), the mid-point of the license plate lower edge heights can be used as a coarse estimate,

$$\mathrm{E}\{H - h\} = 0.70 \text{ m} \quad (25)$$

The corresponding error in estimating the height of the lower license plate edge is therefore

$$\left|\delta\{H - h\}\right| \approx \left|\delta h\right| \le 0.40 \text{ m} \quad (26)$$

In compliance with national highway codes, the camera mounting height $H$ above the ground must

always excede 5 metres [16, 17]. Installing the camera at safe mounting heights results in relative error δh/h which can be easily kept below 10 %, as requested by traffic law enforcement agencies [5].

The contribution of the license plate height uncertainty is by far the largest among all discussed error sources, as shown in Fig. 8. It manifests itself as a constant bias over all image rows (i.e., over all possible positions of the license plate).

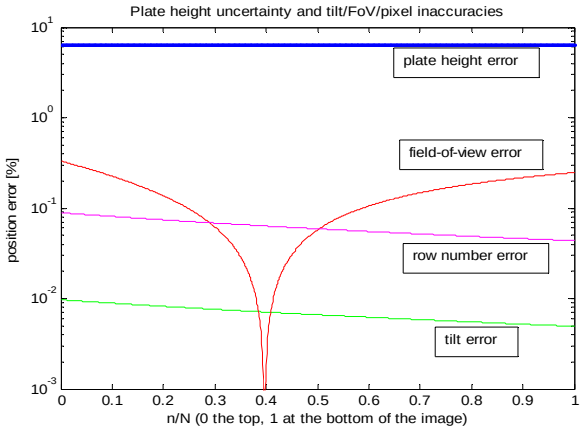


**Fig. 8.** The positioning error over image rows due to various sources, as described in Equations (17), (19), (21) and (26). It is mainly caused by the license plate height uncertainty.

### 3.6. Frame-rate Drift and Speed Error

The error in positioning the license plate.

$$\delta\{Y_R(t_2)-Y_R(t_1)\}= \delta\{h\cdot K(t_2)-h\cdot K(t_1)\}= \left[K(\alpha,\varphi,n_2)-K(\alpha,\varphi,n_1)\right]\delta h + h\left[\delta K(t_2)-\delta K(t_1)\right] \quad (27)$$

where $K(\alpha,\phi,n_p)$ is from Equation (14)

$$K(\alpha,\phi,n_p)=\ldots \frac{\left(2-\frac{n_p}{N_r}\right)\cos\left(\alpha+\frac{\varphi}{2}\right)-\left(1-\frac{n_p}{N_r}\right)\cos\left(\alpha-\frac{\varphi}{2}\right)}{\frac{n_p}{N_r}\cdot\sin\left(\alpha+\frac{\varphi}{2}\right)+\left(1-\frac{n_p}{N_r}\right)\cdot\sin\left(\alpha-\frac{\varphi}{2}\right)} \quad (28)$$

From Equation (27), the relative displacement error is

$$\frac{\delta\{Y_R(t_2)-Y_R(t_1)\}}{Y_R(t_2)-Y_R(t_1)}= \frac{\delta h}{h}+\frac{\delta K(\alpha,\varphi,n_2)-\delta K(\alpha,\varphi,n_1)}{K(\alpha,\varphi,n_2)-K(\alpha,\varphi,n_1)} \quad (29)$$

Consequently, the relative error of the license plate displacement estimate will be limited by

$$\left|\frac{\delta\{Y_R(t_2)-Y_R(t_1)\}}{Y_R(t_2)-Y_R(t_1)}\right| \le \left|\frac{\delta h}{h}\right|+\frac{\max_{n_2}\left|\delta K(\alpha,\varphi,n_2)\right|+\max_{n_1}\left|\delta K(\alpha,\varphi,n_1)\right|}{\left|K(\alpha,\varphi,n_2)-K(\alpha,\varphi,n_1)\right|} \quad (30)$$

The value $K(\alpha,\phi,n_p)$ is monotonically decreasing with $n_p$, i.e., increasing towards the top of the image, as shown in Fig. 9.

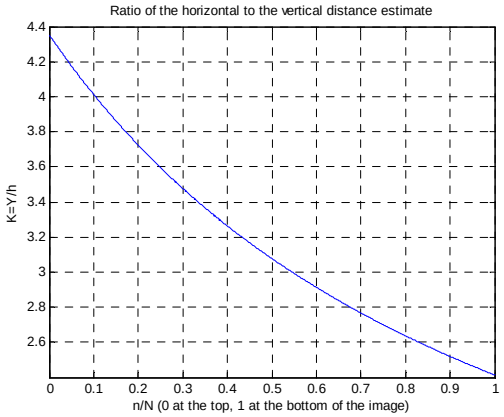


**Fig. 9.** The horizontal distance estimate increases monotonically towards the top of the image ($n_{row}$=0), here expressed as multiple of the vertical distance berween the camera and the licence plate, according to Equation (28). Row numbers are normalized with respect to the total number of rows.

From Fig. 8, the error in estimating the horizontal distance of a vehicle from a camera is at maximum when the vehicle is observed at the top of the image. In Equation (29), this case occurs for the license plate of a departing vehicle successively captured in two top rows, $n_1$=2 and $n_2$=1 (or vice versa, for the approaching vehicle).

Assuming $N_r >> n_p$, a continuous value λ can be used to represent $n_p/N_r$. This value will be practically zero at the top rows of the image, $\lambda_1 \approx \lambda_2 \le 2/N_r \approx 0$. Thus, the maximum error in estimating $K(\alpha,\phi,n_p)$can be derived from partial derivatives in Equations (16), (18) and (20) as

$$\delta K(\lambda_{\max(\delta K)})=\frac{\left|1-2\cos\varphi\right|}{\sin^2(\alpha-\frac{\varphi}{2})}\delta\alpha+\cdots + \frac{\left|2\cos(2\alpha)-1\right|}{2\sin^2(\alpha-\frac{\varphi}{2})}\delta\varphi+\frac{\left|2\sin\frac{\varphi}{2}\cos(2\alpha+\frac{\varphi}{2})\right|}{\sin^2(\alpha-\frac{\varphi}{2})}\delta\lambda \quad (31)$$

where λ corresponds to the first rows, i.e., to the top of the image,

$$\lambda_{\max(\delta K)}=0 \quad (32)$$

At the top of the image, the ratio $K(\alpha,\phi,n_p)$ can be approximated by Taylor series,

$$K(n_p) \approx T(\lambda) = A_0 + A_1\lambda + o(\lambda^2) \tag{33}$$

where

$$A_0 = \frac{\cos\alpha \cdot \cos\frac{\varphi}{2} - 3\sin\alpha \cdot \sin\frac{\varphi}{2}}{\sin\left(\alpha - \frac{\varphi}{2}\right)} \tag{34}$$

and

$$A_1 = 2\sin\frac{\varphi}{2} \cdot \frac{\sin 2\alpha \cdot \sin\frac{\varphi}{2} - \cos 2\alpha \cdot \cos\frac{\varphi}{2}}{\sin^2\left(\alpha - \frac{\varphi}{2}\right)} \tag{35}$$

The error limit in (30) can therefore be approximated as

$$\left|\frac{\delta\{Y_R(t_2) - Y_R(t_1)\}}{Y_R(t_2) - Y_R(t_1)}\right| \le \left|\frac{\delta h}{h}\right| + \frac{2\left|\delta K(\lambda_{\max(\delta K)})\right|}{|A_1|} \text{ i.e., } \tag{36}$$

$$\left|\frac{\delta\{Y_R(t_2) - Y_R(t_1)\}}{Y_R(t_2) - Y_R(t_1)}\right| \le \left|\frac{\delta h}{h}\right| + \ldots$$

$$\frac{\left|2 - 4\cos\varphi\right|\delta\alpha + \left|2\cos(2\alpha) - 1\right|\delta\varphi + \left|4\sin\frac{\varphi}{2}\cos(2\alpha + \frac{\varphi}{2})\right|\delta\lambda}{\left|2\sin\frac{\varphi}{2}\left(\sin 2\alpha \cdot \sin\frac{\varphi}{2} - \cos 2\alpha \cdot \cos\frac{\varphi}{2}\right)\right|}$$

For the tilts and fields of view usually encountered in ALPR cameras, the last term is below 1.4 %. Its variation with respect to the usual tilt and field-of-view ranges is illustrated in Fig. 10.

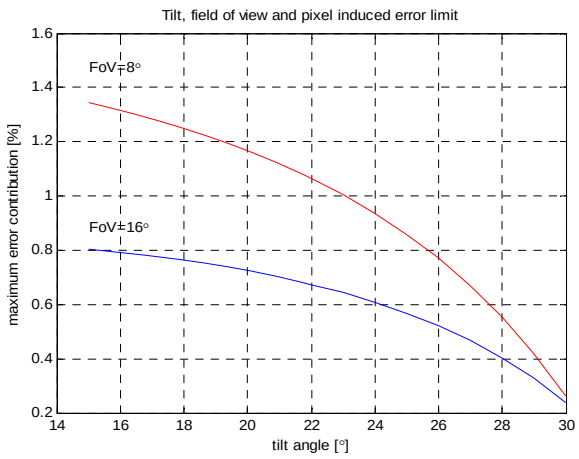


**Fig. 10.** The contribution of non-height parameters to the error limit (the last term in inequality (36) is limited for the camera fields of view and tilts used in practice and comparatively low to the error induced by the uncertainty of the licence plate height.

The limit in (28) is imposed on the vehicle displacement measurement error $Y(t_2)$-$Y(t_1)$, where each position $Y(t)$ is observed in an image frame. The speed of a vehicle can be computed as a product of displacement between successive frames and the frame rate $f$,

$$v(t_2) = \frac{Y_R(t_2) - Y_R(t_1)}{t_2 - t_1} = f \cdot \Delta Y_R(t_2) \tag{37}$$

The speed estimate error is limited as

$$\frac{\delta v}{v} \le \left|\frac{\delta f}{f}\right| + \frac{\delta\{\Delta Y_R\}}{\Delta Y_R} \tag{38}$$

The frame triggering accuracy has also to be taken into account. The frame rate drift in industrial vision cameras for moderate frame rates (10-30 fps) is between 0.1 % and 0.4 %, which is one order of magnitude below the previously discussed error contributions.

From (26), (36) and (38), it is obvious that at sufficient cantilever heights (say h=6 meters), the sum of all errors discussed above never exceeds the allowed discrepancy of 10 % with respect to the more accurate primary measurements.

## 4. Conclusion

In this paper, we proposed an image-based method for measuring the speed of vehicles in accordance with the requirements of the Road Traffic Regulation Act for secondary speed estimates. The method is based on tracking the vehicle license plate using a typical ALPR camera. The largest error contributor is the uncertainty of vertical separation between the camera and the license plate, i.e., the uncertainty of the license plate height above the ground. Assuming the above uncertainty of ±0.4 cm over a say 6.7 meter camera height with respect to the ground (i.e., 6 meters above the assumed license plate position), this contribution is δh/h=6.7 %. The camera angle and pixel error δ(ΔK)/(ΔK) derived in the right-hand term of inequality (36) and illustrated in Fig. 10 is below 1.4 % for a large range of tilts and fields of view used in practice. The frame rate error $\delta f/f$ is below 0.4 %. Consequently, the cumulative error limit would not exceed 8.5 % for the above range of parameters, which is comfortably below the 10 % limit requested by regulators for the secondary speed estimate.

## Acknowledgements

This work was supported by the European Commission, grant agreement no: 611362, FP7-PEOPLE, "Industry-Academia Research on Three-dimensional Image Sensing for Transportation".

## References


[1]. Department for Transport of the United Kingdom, Contributory Factors to Reported Road Accidents, Article in, Reported Road Casualties Great Britain, 2010, DfT 2011, (https://www.gov.uk/government/uploads/system/uploads/attachment_data/file/463043/rrcgb2014-02.pdf).

[2]. Royal Society for the Prevention of Accidents, Speed Cameras, December 2011, (http://www.rospa.com/roadsafety/advice/drivers/speed/cameras/).

[3]. C. Willson, C. Willis, J. K. Hendrikz, R. Le Brocque and N. Bellamy, Speed cameras for the prevention of road traffic injuries and deaths (Review), Cochrane Database of Systematic Reviews 2010, Issue 10, Art. No. CD004607. (http://www.roadsafetyobservatory.com/Evidence/Details/11158).

[4]. C. Willson, C. Willis, J. K. Hendrikz, R. Le Brocque and N. Bellamy, Speed enforcement detection devices for preventing road traffic injuries, *Cochrane Database of Systematic Reviews 2006*, Issue 2, 19 April 2006. (http://www.roadsafetyobservatory.com/Evidence/Details/11158).

[5]. Association of Chief Police Officers of England, Wales and Northern Ireland, Guide for the operational use of speed and red-light offence detection technology, December 2011 (http://library.college.police.uk/docs/ACPO/Speed-and-red-light-technology-2011.pdf).

[6]. The Sunday Times Driving Web Portal (http://www.driving.co.uk/news/new-road-markings-mean-slow-down-for-average-speed-traps/).

[7]. Safer Roads Web Portal (http://www.saferroads.org/archive/camera-site-stats/).

[8]. Directive of the Council dated 20th March 1970 concerning the harmonization of the legislation of member countries relating to the positioning and installation of the rear number plate of motor vehicles and their trailers, 70/222/CEE, *Journal Officiel des Communautés Européennes,* Issue L76, 6 April 1970, pp. 25-6.

[9]. 1. Z. Sun, G. Bebis, R. Miller, On-Road Vehicle Detection: A Review, *IEEE Transactions on Pattern Analysis and Machine Vision,* Vol. 28, No. 5, 2006, pp. 694-711.

[10]. N. K. Kanhere, Automatic Camera Calibration Using Pattern Detection for Vision-Based Speed Sensing, *Transportation Research Board Annual Meeting*, Washington, D. C., January 2008.

[11]. M. Dubska, J. Sochor, A. Herout, Automatic Camera Calibration for Traffic Understanding, in *Proceedings of the British Machine Vision Conference*, Nottingham, September 2014.

[12]. M. Dubska et al., Automatic Camera Calibration for Traffic Understanding, *IEEE Transactions on Intelligent Transportation Systems*, Vol. 16, Issue 3, June 2015, pp. 1162 – 1171.

[13]. V. Lukic et al., Stereoscopic vehicle speed measurement - System calibration and synchronization errors analysis, in *Proceedings of the International Conference on 3D Imaging (IC3D)*, Liege, 2011, pp. 1-6.

[14]. Commission Regulation (EU) No 1003/2010, subparagraphs 1. 2. 1. 4. 1 and 1. 2. 1. 4. 2, *Official Journal of the European Union,* Legislation, L 291, Vol. 53, 9 November 2010. (http://eur-lex. europa. eu/legal-content/EN/TXT/?uri=CELEX:32010R1003).

[15]. G. P. Stein, Accurate internal camera calibration using rotation, with analysis of sources of error, in *Proceedings of the 5th International Conference on Computer Vision,* Cambridge MA, 1995, pp. 230 – 236.

[16]. Department for Transport of the United Kingdom, Design Manual for Roads and Bridges (DMRB), Volume 2, Highways Structures: Design (Substructures and Special Structures), Section 2 Special Structures, Part 4: BD 51/14, Portal and Cantilever Sign/Signal Gantries, Paragraph 7. 6, May 2014. (www.standardsforhighways.co.uk/ha/standards/dmrb/vol2/section2/bd5114.pdf).

[17]. Department for Transport of the United Kingdom, Design Manual for Roads and Bridges (DMRB), Vol. 6, Road geometry, Section 1, Part 2, TD 27/05, Cross-sections and headrooms, Table 6-1, February 2005. (http://www.standardsforhighways.co.uk/ha/standards/ghost/dmrb/vol6/section1/td2705.pdf).


2016 Copyright ©, International Frequency Sensor Association (IFSA) Publishing, S. L. All rights reserved. (http://www.sensorsportal.com)